Progress In Electromagnetics Research B, Vol. 55, 87–114, 2013

A MULTI-FIDELITY BASED ADAPTIVE SAMPLING OPTIMISATION APPROACH FOR THE RAPID DESIGN OF DOUBLE-NEGATIVE METAMATERIALS

Patrick J. Bradley

RF & Microwave Research Group, School of Electrical Electronic and Communications Engineering, University College Dublin, Ireland

Abstract—Due to the increasing complexity of metamaterial geometric structures, direct optimisation of these designs using conventional approaches, such as Gradient-based and evolutionary algorithms, are often impractical and limited. This is in part due to the inherently high computational cost associated with running multiple expensive high-fidelity full-wave simulations, commonly required to optimise the constitutive parameters of a single metamaterial particle. In order to alleviate this issue, we propose an efficient optimisation approach which exploits the Co-Kriging methodology, such that we can successfully couple varying levels of discretisation and solver accuracy obtained from a 3d full-wave numerical solver suite. In contrast to other optimisation strategies, we investigate the improvement in efficiency of optimisation through the use of the LOLA-Voronoi, in conjunction with Expected Improvement and the embedding of a trust-region framework within our optimisation algorithm, to accelerate the convergence of Co-Kriging. Finally, the effectiveness of the outlined algorithm will be demonstrated by a quantitative evaluation of the performance of optimised planar 2D negative index of refraction structures.

1. INTRODUCTION

The ability to independently tailor the electric and magnetic response of sub-wavelength geometric structures to electromagnetic energy, has provided the opportunity for designers to create fully customised artificial materials termed Metamaterials. These structures allow for fully tuneable material properties that can be engineered to have

Received 10 July 2013, Accepted 23 September 2013, Scheduled 24 September 2013
* Corresponding author: Patrick J. Bradley (bradleypatrickj@gmail.com).

either positive or negative values of permittivity ϵ, permeability μ and consequently the ability to achieve a negative index of refraction n (NIR) [1, 2].

The macroscopic properties of metamaterials are harnessed by engineering the geometric dimensions of the constituent particles. Due to the increased complexity of these geometric structures, exacerbated by the increased interest in generating inhomogeneous and anisotropic metamaterials, direct optimisation of these designs using conventional approaches such as Gradient-based [3] and Genetic algorithms [4] are often impractical and limited. This is in part due to the inherently high computational cost associated with running multiple expensive high-fidelity (primary) full-wave simulations, commonly required to optimise the constitutive parameters of a single metamaterial particle, and the underlying numerical noise that can adversely affect the simulation-driven optimisation cycle.

Thus, a key challenge is to be able to perform global optimisation using physics-based simulations in an efficient manner so as to allow these methods to be used within the short time-scales of conceptual design. As a consequence, alternative measures which make economical use of the primary data must be considered, in conjunction with surrogate models that can incorporate low fidelity (auxiliary) data within the framework of a global optimisation strategy. Preferably, the auxiliary model should be a reasonably accurate representation of the primary model, computationally inexpensive to evaluate and amenable to optimisation. A wide variety of possible auxiliary models are available and are largely dependant on the type of system been modelled. Typically, these include simplified physics models, numerical models evaluated at varying levels of discretisation and/or converged to contrasting degrees of accuracy, Reduced Order Models (ROMs), response surfaces models and artificial neural networks. Indeed, while analytical methods can be formulated for limited classes of metamaterial structures, they are often unable to accurately predict the macroscopic behaviour of metamaterials. More importantly they may not be acceptable or even desirable in an automated design driven optimisation cycle.

An optimisation design space with widely set bounds can be searched effectively using local surrogate based methodologies, such as space and manifold mapping [5, 6] if the design space is uni-modal. However, it must be assumed that there may be local basins of attraction, with the prospect that the objective function multi-dimensional landscape is highly nonlinear. As such, a global search is required to increase the chances of isolating the global optimum. Commonly used global approximation surrogate models

such as Kriging [7], Radial Basis Functions [8] (RBFs) and polynomial response surface model [9] (RSM), attempt to approximate the primary objective function landscape, which in turn are inexpensive to evaluate within an optimisation cycle. These models may be realised by sampling the primary objective landscape at a large number of sites, in order to assimilate the underlying salient feature of the landscape. To achieve the right balance between exploitation and exploration of the design space, these approaches must be coupled with a credible infill criterion. Accurately modelling suboptimal regions is not essential in a global optimisation approach, while exploiting the surrogate model before the design space has been explored sufficiently may lead to the global optimum lying undiscovered. This trade off can be successfully achieved with the Expected Improvement (EI) criteria [10, 11], which determines the next infill point by calculating the amount of improvement we can expect compared to the best observed objective value. Based on the expected problem dimensionality, complexity and the form of infill strategy we wish to pursue, Kriging is a natural selection that makes the least amount of assumptions regarding the underlying landscape and provides the potential for the most accurate predication [11, 12].

However, a more efficient use of the primary simulations can be conceived, the Co-Kriging [10, 13], which uses auxiliary simulations to build a statistical approximation of the objective landscape. If the sampled points are reasonably uniformly spread, then the method should be accurate enough to guide the search towards promising areas of the landscape. The Co-Kriging essentially couples a relatively small amount of primary data to improve the accuracy of the model by correcting the output of the auxiliary model. This ensures that the computation time is drastically reduced in finding the global optimum, by proving a more exhaustive search of the auxiliary model to seed a narrower search using the primary simulations. In order to limit the number of data points in an optimal manner while maximising the model accuracy, we employ an adaptive sampling algorithm, the LOcal Linear Approximation (LOLA)-Voronoi [14]. This algorithm iteratively selects data points based on the previous iterations to efficiently distribute new samples in areas that highlight the most salient features of the design space. In addition, we also employ a trust-region inspired methodology [15] that ensures the convergence of the Co-Kriging scheme to a solution of the primary problem. This is achieved by providing a systematic response to situations in which an optimisation phase preformed gives a poor prediction of the primary model actual behaviour.

The motivation for this work is to consider for the first time the

application Co-Kriging to the topology optimisation of metamaterial structures. In addition, we evaluate what additional amendments are required to result in an efficient and robust automated global optimisation scheme that requires no prior knowledge of the problem. In particular, we exploit the co-Kriging methodology to successfully couple varying levels of discretisation and solver accuracy gleaned from a 3d full-wave numerical solver suite. In contrast to other optimisation strategies, we investigate the improvement in efficiency of optimisation through the use of the LOLA-Voronoi, in conjunction with EI and the embedding of a trust-region (TR) framework within our optimisation algorithm, to accelerate the convergence of Co-Kriging. Finally, the effectiveness of the outlined algorithm will be demonstrated by a quantitative evaluation of the performance of optimised planar 2D NRI structures in the GHz regime.

1.1. Planar 2D Negative Refractive Index (NRI) Metamaterials

Initial efforts to harvest NRI materials were realised by designing structures consisting of split-ring resonators (SRRs) in combination with electric inductive-capacitive (ELC) resonators [16] (D1)[†] or wire arrays [1, 2] (D2). However, there were fundamental limitations in both the design and manufacturability of such approaches. This is a result of the restrictive orientation of the excitation field relative to the SRR design required to produce a NRI response which is further complicated by the bi-anisotropy nature of these structures. Accordingly, the incident magnetic field must be perpendicular to the SRRs plane to produce a negative μ, with the electric field parallel to the wire array to obtain a negative ϵ via a plasmonic response.

By a procedure of continuous transformation, these designs have been simplified to a pair of carefully aligned metallic strips (D3) separated by a dielectric spacer, which overcomes the limiting restriction imposed by the original design [17]. The capability of paired metallic strips to provide a NRI response, stems from the hybridisation of the plasmonic eigenmodes of each individual strip that results in two separate eigenmodes with opposite symmetry. This mode hybridisation is due to near-field interactions between the paired strips that leads to the resonance splitting, subject to an in-plane electric and magnetic excitation [18]. A Lagrangian formulation with a quasi-static dipole-dipole interaction model has been successfully used to study the hybridisation effects in SRR arrays [19]. In these resonator systems, it is found that both electric and magnetic dipoles contribute to inter-

[†] Where D1–D6 refers to specific designs.

resonator coupling, and the coupling efficiency depends on the distance and relative orientation among the resonators.

The high energy or anti-bonding mode, $|\omega_+\rangle$ is characterised by in-phase current oscillations associated with a resonant electric response and a negative ϵ regime, while the opposite is true for the bonding of low energy $|\omega_-\rangle$ magnetic resonance [19]. The design of NRI metamaterials consists of preserving an overlap between these two modes, where the frequency split $\Delta\omega = \omega_+ - \omega_- \approx \kappa\omega_0$ is proportional to the coupling strength κ [19]. As the tuning of the two resonances by a single geometric parameter l (the length of the strip) is not feasible, the eigenmode overlap is obtained by adjusting either the spacer or the alignment of the paired metallic strips [20]. The lower resonance frequency in particular is extremely sensitive to the characteristics of the gap between the wires, making the cut wire lattice difficult to design accurately.

An alternative approach, to lower the electric resonance in the magnetic negative μ region, is to increase the inter-particle capacitance by increasing the width of the strip ends to produce the classic dogbone shape [21] (D4). This increase in capacitance can only be obtained by strongly reducing the spacing between two consecutive strips, which will be limited according to the fabrication technology. Other theoretical proposals include combining continuous strips (D5) to produce negative ϵ due to a plasmonic response with the negative μ produced by the metallic strip pair [22]. However, these strip lattices exhibit strong spatial dispersion regardless of the wavelength relative to the lattice spacing, and as a consequence of the natural scaling of the effective permittivity with the unit cell dimensions, makes these designs problematic.

To mitigate this sensitivity, several variants of the strip structure have been introduced. In the context of a proven robust and scalable design the fishnet structure [23–25] Figure 1 (D6), has provided significant progress in the realisation of NRI at higher frequencies well into the THz range. The fishnet design consists of a pair of metal films separated by a dielectric layer, with an array of periodically placed rectangular, circular, elliptical or cross shaped holes penetrating the metallic layers. Conceptually this design is derived from extending the paired strip end of D5 to join the continuous wire arrays to produce a continuously connected network.

Recently, a further possibility to accomplish a NRI response at both high frequencies and high dimensions was realised based on an isolated pair of ELC components combined with a metallic strip [26] Figure 1 (D7). Under normal incidence, the fundamental electrically excited resonant eigenmodes $|\omega_{1,2}\rangle$ of the single ELC undergo a

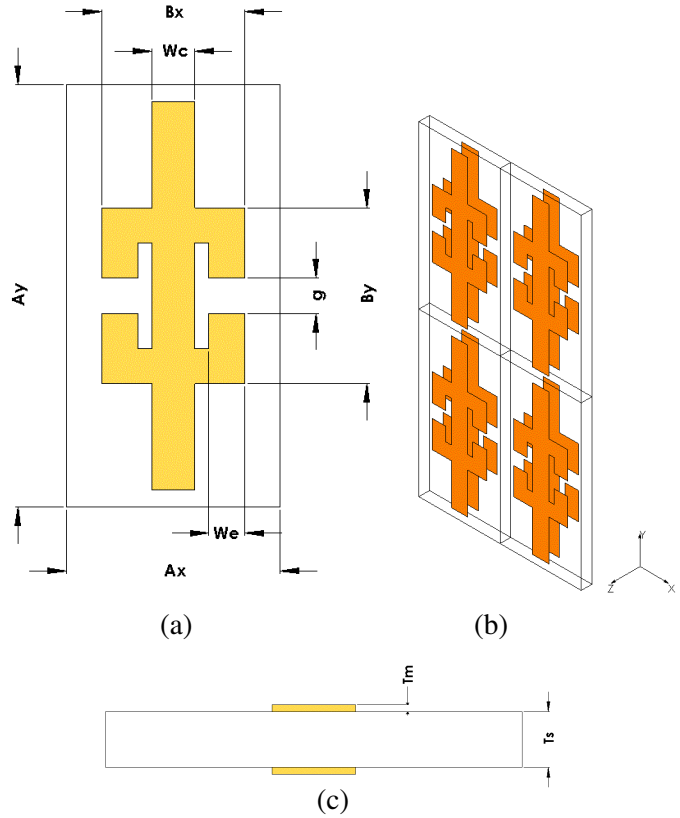

Figure 1. (a) Schematic representation of the 2D mode hybridisation metamaterial NIM design, (b) isometric view of a layer of the metamaterial formed by a periodic array of patterned metallic double layers separated by a thin dielectric substrate and (c) bottom view of the proposed structure.

hybridisation, where the coupling between the paired ELCs lifts the degeneracy of the single ELC mode into two separate eigenmodes. As with D4 these modes exhibit opposite symmetry and display $|\omega_{e2}\rangle > |\omega_{m2}\rangle > |\omega_{e1}\rangle > |\omega_{m1}\rangle$, where e, m refers to the type of resonance. Unlike D4 where the overlap between the negative ϵ from $|\omega_{e1}\rangle$ and negative μ from $|\omega_{m2}\rangle$ is achieved by adjusting the overlap between the paired strips, the same effect can be achieved with ease by adjusting the ELC geometric parameters. Indeed this design alleviates the limitation of D4 by providing additional flexibility in the design of

a NRI response, with the parameter l_c providing sufficient modulation to ensure the overlap between the hybridized modes.

Nevertheless, these different classes of designs D1–D6, remain very sensitive to their constituent geometric parameters and lattice spacing, implying the need for careful selection and optimisation of these parameters.

1.2. Retrieval of Effective Constitutive Parameters

In order to conceptualise the complex propagation characteristics of the local field structure around metamaterial elements, one needs to average the local field charge and current distribution which yields a macroscopic interpretation of the inhomogeneous composites [27]. This homogenisation procedure relies on the applied fields having a spatial variation on a scale significantly larger than the scale of the composite particles and the period of the lattices. By replacing the inhomogeneous structure with a continuous material and restricting our analysis to that of a linear polarized incident wave, the effective permittivity ϵ and permeability μ of the inhomogeneous slab can be characterised. Based on Nicolson and Ross [28] (NR) these effective parameters can be retrieved by calculating the scattering parameters from a material slab and comparing them to analytical expression for a homogeneous slab of the same thickness d. Assuming a time harmonic time dependence, the reflection Γ and transmission T coefficients are given by

$$\Gamma = K \pm \sqrt{K^2 - 1}, \quad T = \frac{S_{21}}{1 - S_{11}\Gamma} \tag{1}$$

$$K = \frac{S_{11}^2 - S_{21}^2 + 1}{2S_{11}}, \quad \frac{1}{\Lambda} = \frac{-j}{2\pi d}\ln(T) \tag{2}$$

Subsequently ϵ, μ and the complex effective refractive index n can be extracted from the Γ and T coefficients

$$\epsilon_r = \frac{\lambda_0^2\left(1/\Lambda^2\right)}{\mu_r}, \quad \mu_r = \lambda_0 \frac{1}{\Lambda}\left(\frac{1+\Gamma}{1-\Gamma}\right), \quad n = \pm\sqrt{\epsilon\mu} \tag{3}$$

where λ_0, Λ are the free space and sample wavelengths, respectively. The resultant retrieved material parameters must be physically reasonable and are subject to the following restrictions

$$\|\Gamma\| =\leq 1, \quad n'' \geq 0 \tag{4}$$

required by causality for passive materials [27, 29], where $(\cdot)'$ and $(\cdot)''$ denote the real and imaginary part operators, respectively. However, ambiguity can still arise in the definition of the constitutive parameters

due to the multi-valued solution to the branching problem in the logarithmic function (see Equation (2)), stemming from the complex exponential propagation factor in the transmission coefficient. To resolve this phase ambiguity, we use a conceptually simple routine recently published [30] which recast the logarithmic function as

$$\frac{1}{\Lambda} = \begin{cases} \frac{1}{2\pi d}\left(-j\ln\|T\| + \phi\right) & \text{if } -\pi < \phi < \pi \\ \frac{1}{2\pi d}\left(-j\ln\|T\| + \phi + 2m\pi\right) & \text{otherwise} \end{cases} \tag{5}$$

where m is an integer denoting the branch index. The choice of m is determined by examining the behavior of the phase of T at which the phase jumps from $-\pi$ to π. Based on this information, the unwrapping method introduces the phase component $2m\pi$ into T to ensure that the logarithmic function will be single valued and continuous at $\|T\|$[‡].

In addition to correctly determining the branch indices, in order to remove any ambiguity in the material retrieval process, one must also be careful in determining the location of the effective boundaries between the metamaterial slab and air. Due to the effect of the scattered field produced by the resonant metamaterial structure, an effective boundary must be introduced which indicates the distance at which the reflected wave behaves like a plane wave. Based on the fact that the impedance of a homogenous slab of material does not depend on its thickness, the effective boundary is determined as the location where the impendence difference between two slabs of different thickness is minimised [31]. It should be noted that the topic of parameter extraction is still evolving with several alternative schemes having been postulated in recent years (see [31, 32]).

1.3. Co-Kriging

Co-Kriging is a multivariate enhancement to the geostatistical method of Kriging [7], that attempts to build an approximation of a function that is expensive to evaluate, through coupling cheap low fidelity data (auxiliary) with a small amount of high fidelity data (primary) [13]. The auxiliary is cross correlated with the primary and is usually sampled more frequently and regularly, thus allowing estimation of unknown points using both data sets globally.

A brief overview of Co-Kriging will be given here with the reader directed to [12, 13] for more detailed information on this approach. Although multi sets of variable-fidelity data can be considered, we are only interested in two data sets, that of the primary with values $\mathbf{y}_p$ at

[‡] It should be noted that when the phase of T remains confined to the interval $[-\pi, \pi]$ there is no branching problem and the standard extraction procedure is able to correctly retrieve the constitutive parameters.

points $\mathbf{X}_p$ and auxiliary, $\mathbf{y}_a$ at points $\mathbf{X}_a$ ($\mathbf{X}_p \subset \mathbf{X}_a$). These data sets are concentrated to give the combined set of points

$$\mathbf{X} = \begin{pmatrix} \mathbf{X}_a \\ \mathbf{X}_p \end{pmatrix} = \left(\mathbf{x}_a^{(1)}, \ldots, \mathbf{x}_a^{(n_a)}, \mathbf{x}_p^{(1)}, \ldots, \mathbf{x}_p^{(n_p)}\right)^T \tag{6}$$

$$\begin{aligned} \mathbf{y} &= \begin{pmatrix} \mathbf{y}_a(\mathbf{X}_a) \\ \mathbf{y}_p(\mathbf{X}_p) \end{pmatrix} \\ &= \left(y_a\left(\mathbf{x}_a^{(1)}\right), \ldots, y_a\left(\mathbf{x}_a^{(n_a)}\right), y_p\left(\mathbf{x}_p^{(1)}\right), \ldots, y_p\left(\mathbf{x}_p^{(n_p)}\right)\right)^T. \end{aligned} \tag{7}$$

To construct a Co-Kriging model, the auto-regressive formulation of Kennedy and O'Hogan [33] is used

$$Z_p(\mathbf{x}) = \rho Z_a(\mathbf{x}) + Z_d(\mathbf{x}),\ \mathrm{cov}\left\{Z_p\left(\mathbf{x}^{(i)}\right),\ Z_a(\mathbf{x}) | Z_a\left(\mathbf{x}^{(i)}\right)\right\} = 0\ |^{\forall \mathbf{x} \neq \mathbf{x}^{(i)}} \tag{8}$$

where $Z_a(\cdot)$ and $Z_p(\cdot)$ are Gaussian processes that represents the local features of the auxiliary and primary data. The above auto-regressive model approximates the primary as the sum of the auxiliary, scaled by a constant factor ρ plus a Gaussian process $Z_d(\cdot)$ representing the difference between $\rho Z_a(\cdot)$ and $Z_p(\cdot)$. As with the Kriging approach, the observed data is correlated with each other using the Kriging basis function expression

$$\Psi\left(\mathbf{x}^{(i)}, \mathbf{x}^{(j)}\right) = \exp\left(-\sum_{k=1}^{n} \theta_k \left\|\mathbf{x}_k^{(i)} - \mathbf{x}_k^{(j)}\right\|_k^p\right) \tag{9}$$

where θ is a width parameter controlling the spatial extent of a sample point's influence, and p is a parameter controlling the local smoothness[§]. A key attribute of surrogate modelling is the ability to modify the co-Kriging formulation such that the data can be regressed appropriately to filter out any noise. Any anomalies in the data can make optimisation difficult and might mislead an infill criterion into poor design areas. For multi-fidelity analysis different levels of filtering may be required. This is useful when our sampled data has an element of systematic error, due to for example, different levels of discretisation and or convergence [34, 35]. In the augmented Co-Kriging formulation, regression constants λ_a, λ_p are added to the leading diagonal of the correlation matrices to give

$$\mathbf{C} = \begin{pmatrix} \sigma_a^2\left\{\Psi_a(\mathbf{X}_a, \mathbf{X}_a) + \mathbf{I}_{(n_a \times n_a)}\lambda_a\right\} & \rho\sigma_a^2 \Psi_a(\mathbf{X}_a, \mathbf{X}_p) \\ \rho\sigma_a^2 \Psi_a(\mathbf{X}_p, \mathbf{X}_a) & \begin{array}{l}\rho^2\sigma_a^2\left\{\Psi_a(\mathbf{X}_p, \mathbf{X}_p) + \mathbf{I}_{(n_p \times n_p)}\lambda_a\right\} \\ +\sigma_d^2\left\{\Psi_d(\mathbf{X}_p, \mathbf{X}_p) + \mathbf{I}_{(n_p \times n_p)}\lambda_p\right\}\end{array} \end{pmatrix} \tag{10}$$

[§] We assume that there will not be any discontinuities and use $p = 2$, thus reducing the complexity associated with tuning the hyper-parameters.

where σ^2 is the processes variance of $\mathbf{Y}(\cdot)$ and Ψ the spatial correlation function. As our auxiliary data is considered independent of the primary, we can calculate the unknown parameters μ_a, σ_a^2, λ_a, and θ_a (hyper-parameters) by maximising the ln-likelihood

$$-\frac{n_a}{2}\ln\left(\sigma_a^2\right) - \frac{1}{2}\ln\left|\det\left(\Psi_a\left(\mathbf{X}_a,\mathbf{X}_a\right)+\lambda_a\mathbf{I}\right)\right| \tag{11}$$

where the variance and mean are given by maximum likelihood estimates (MLEs)[‖]

$$\sigma_a^2 = \frac{\left(\mathbf{y}_a-\mathbf{1}\mu_a\right)^T\left(\Psi_a+\lambda_a\mathbf{I}\right)^{-1}\Psi_a\left(\Psi_a+\lambda_a\mathbf{I}\right)^{-1}\left(\mathbf{y}_a-\mathbf{1}\mu_a\right)}{n_a} \tag{12}$$

$$\mu_a = \frac{\mathbf{1}^T\left(\Psi_a+\lambda_a\mathbf{I}\right)^{-1}\mathbf{y}_a}{\mathbf{1}^T\left(\Psi_a+\lambda_a\mathbf{I}\right)^{-1}\mathbf{1}}. \tag{13}$$

Similarly, the parameters μ_d, σ_d^2, θ_d and the scaling factor ρ associated with the difference model

$$\mathbf{d} = \mathbf{y}_p - \rho\mathbf{y}_a\left(\mathbf{X}_p\right) \tag{14}$$

are calculated by maximising the ln-likelihood of d, given by

$$-\frac{n_p}{2}\ln\left(\sigma_d^2\right) - \frac{1}{2}\ln\left|\det\left(\Psi_d\left(\mathbf{X}_p,\mathbf{X}_p+\lambda_p\mathbf{I}\right)\right)\right| \tag{15}$$

yielding MLEs of

$$\sigma_d^2 = \frac{\left(\mathbf{d}-\mathbf{1}\mu_d\right)^T\left(\Psi_d+\lambda_p\mathbf{I}\right)^{-1}\Psi_d\left(\Psi_d+\lambda_p\mathbf{I}\right)^{-1}\left(\mathbf{d}-\mathbf{1}\mu_d\right)}{n_p} \tag{16}$$

$$\mu_d = \frac{\mathbf{1}^T\left(\Psi_d+\lambda_p\mathbf{I}\right)^{-1}\mathbf{d}}{\mathbf{1}^T\left(\Psi_d+\lambda_p\mathbf{I}\right)^{-1}\mathbf{1}}. \tag{17}$$

Equations (11) and (15) cannot be reliably solved using a local optimisation technique. As such a suitable global search routine is typically used[¶].

With the parameters estimated, the Kriging and Co-Kriging predication at an unknown $\mathbf{x}$ is now given by

$$\widehat{y}_a\left(\mathbf{x}^{(n_a+1)}\right) = \mathbf{1}\mu_a + \Psi_a\left(\Psi_a+\lambda_a\mathbf{I}\right)^{-1}\left(\mathbf{y}_a-\mathbf{1}\mu_a\right) \tag{18}$$

$$\widehat{y}_p\left(\mathbf{x}^{(n_p+1)}\right) = \mathbf{1}\mu + \mathbf{c}^T\mathbf{C}^{-1}\left(\mathbf{y}-\mathbf{1}\mu\right) \tag{19}$$

[‖] Ψ_a will now be shorthand for $\Psi_a(\mathbf{X}_a,\mathbf{X}_a)$, similarly $\Psi_d = \Psi_d(\mathbf{X}_p,\mathbf{X}_p)$.

[¶] It should be noted that for high dimensional data sets, $d > 10$, a substantial increase in computational time can occur and techniques by [36] will be required to efficiently circumvent this cost. Further reductions in time can be achieved by keeping the hyper-parameter θ_c constant over several iterations. This has be shown to have a limited effect on the overall accuracy of the approximation.

where

$$\mathbf{c} = \begin{pmatrix} \rho\sigma_a^2\Psi_a\left(\mathbf{X}_a, \mathbf{x}^{(n+1)}\right) \\ \rho^2\sigma_a^2\Psi_a\left(\mathbf{X}_p, \mathbf{x}^{(n+1)}\right) + \sigma_d^2\Psi_d\left(\mathbf{X}_p, \mathbf{x}^{(n+1)}\right) \end{pmatrix} \tag{20}$$

$$\mu = \mathbf{1}^T\mathbf{C}^{-1}\mathbf{y}/\mathbf{1}^T\mathbf{C}^{-1}\mathbf{1}. \tag{21}$$

The estimated mean squared error (MSE) corresponding to the predictors is subsequently given by

$$s_a^2(\mathbf{x}) = \sigma_a^2\left[1 - \Psi_a^T\Psi_a^{-1}\Psi_a + \frac{1 - \mathbf{1}^T\Psi_a^{-1}\Psi_a}{\mathbf{1}^T\Psi_a^{-1}\mathbf{1}}\right] \tag{22}$$

$$s_p^2(\mathbf{x}) = \rho^2\sigma_a^2 + \sigma_d^2\mathbf{c}^T\mathbf{C}^{-1}\mathbf{c}. \tag{23}$$

1.4. Infill Criteria

The success and failure of surrogate based optimisation rests on the correct choice of model and infill criteria. Global based optimisation must find the right balance between exploitation and exploration of the design space. Accurately modelling suboptimal regions is not essential in a global optimisation approach. However, exploiting the surrogate model before the design space has been explored sufficiently may lead to the global optimum lying undiscovered. By modelling the uncertainty in the predication by considering it as the realisation of a Gaussian random variable $Y(\mathbf{x})$ with mean $\widehat{y}(\mathbf{x})$ (Equations (18), (19)) and variance $s^2(\mathbf{x})$ (Equations (22), (23)), an infill criteria can be constructed which balances the values of $\widehat{y}(\mathbf{x})$ and $s^2(\mathbf{x})$. This trade off can be successfully achieved with the Expected Improvement (EI) criteria [10, 11, 13, 37] which determines the next infill point by calculating the amount of improvement we can expect compared to the best observed objective value $\min\{\mathbf{y}_p\}$. While a maximising EI infill process will eventually find the global optimum, its convergence can be slow. Thus it is necessary to couple this approach with alternative measures to ensure convergence in an accelerated framework. Such measures will be discussed in the following sections.

1.5. Adaptive Sampling Plans

In order to limit the number of data points in an optimal manner while maximising model accuracy, we employ an adaptive sampling algorithm the LOcal Linear Approximation (LOLA)-Voronoi [14]. This algorithm iteratively selects data points, based on the previous iterations, to efficiently distribute new samples into areas highlighting the most salient features of the design space. This is achieved by balancing the trade off between exploring regions of design space not

yet identified with exploitation of regions which are highly dynamic. This process starts with an initial design of experiment (DOE) sample data set, such as the Latin Hypercube (LHC) sampling technique, and uses the maximum optimality criterion of Morris and Mitchell [38] in order to achieve uniform coverage of the design space[+]. The density of this data set is then estimated by computing an approximation of the Voronoi tessellation of the entire design space. These samples are then ranked based on the Voronoi cell size which is indicative of whether this region is under-sampled. While this ensures that no region is left permanently under-sampled, an additional measure, the LOLA, is required to sample highly dynamic regions. The LOLA component estimates the gradient at each sample location $\mathbf{x}^{(r)}$, based on a set of neighboring samples $\mathbf{N}(\mathbf{x}^{(r)}) = (\mathbf{x}^{(r1)}, \mathbf{x}^{(r2)}, \ldots, \mathbf{x}^{(rm)})$

$$\begin{aligned}
\nabla y\left(\mathbf{x}^{(r)}\right) &= \begin{pmatrix} \frac{\delta y\left(\mathbf{x}^{(r)}\right)}{\delta x_1^{(r)}} \\ \frac{\delta y\left(\mathbf{x}^{(r)}\right)}{\delta x_2^{(r)}} \\ \vdots \\ \frac{\delta y\left(\mathbf{x}^{(r)}\right)}{\delta x_d^{(r)}} \end{pmatrix} \\
&= \begin{pmatrix} x_1^{(r1)} - x_1^{(r)} & x_2^{(r1)} - x_2^{(r)} & \ldots & x_d^{(r1)} - x_d^{(r)} \\ x_1^{(r2)} - x_1^{(r)} & x_2^{(r2)} - x_2^{(r)} & \ldots & x_d^{(r2)} - x_d^{(r)} \\ \vdots & \vdots & \ddots & \vdots \\ x_1^{(rm)} - x_1^{(r)} & x_2^{(rm)} - x_2^{(r)} & \ldots & x_d^{(rm)} - x_d^{(r)} \end{pmatrix}^{-1} \\
&\quad \begin{pmatrix} y\left(\mathbf{x}^{(r1)}\right) \\ y\left(\mathbf{x}^{(r2)}\right) \\ \vdots \\ y\left(\mathbf{x}^{(rm)}\right) \end{pmatrix}. \qquad (24)
\end{aligned}$$

where $m = 2d$ and d is dimension size. Having estimated the gradient by fitting a hyperplane though the sample point $\mathbf{x}^{(r)}$ based on its m neighbours in a least squared sense, the local nonlinearity can be quantified from the normal of the hyperplane given by

$$E\left(\mathbf{x}^{(r)}\right) = \sum_{k=1}^{m} \left\| y\left(\mathbf{x}^{(rk)}\right) - \left(y\left(\mathbf{x}^{(r)}\right) + \nabla y\left(\mathbf{x}^{(r)}\right)\left(\mathbf{x}^{(rk)} - \mathbf{x}^{(r)}\right)\right) \right\|. \quad (25)$$

[+] Pre-optimised LHC designs are available online which will provide better space-filling properties than those created using the maximum optimality criterion above and will significantly reduce the computational cost of producing an optimum sample set.

Data points with a large deviation indicate a region in the design space where the data is varying more rapidly and will require a proportional increase in samples within this region. In regions where the function is almost linear, the output is easily predicted and will result in a low LOLA value. Combining the Voronoi and LOLA criteria into one metric, provides an optimal approach that can identify locations for additional points in a robust and efficient manner.

1.6. Constraints

Having considered the role of EI in determining new infill points, we must now discuss how to effectively include constraints in the optimisation procedure [12, 39]. To ensure that the objective function is not unfairly penalised in the wrong areas due to a deceptive constraint function, a probabilistic approach will be factored into the calculation of the EI expectation. As with the objective function, the constrained function is modelled by a Gaussian process based on the same sampled data. Using this model to ensure that a design is feasible, we calculate the probability of the predication being greater than the constraint limit [12]. We can couple these results with the EI of the objective function to formulate a Constrained Expected Improvement (CEI). As before, the next infill point will be calculated by maximising this coupled expression to provide a new infill point that both improves on the current best point and is also feasible.

1.7. Trust Radius (TR)

In many situations maximising CEI will prove to be the best route to finding the global optimum. However, it may converge very slowly if the optimum is deceptively positioned. It is therefore prudent to implement a procedure that ensures convergence of the algorithm to a solution of the primary problem. Based on the TR methodology [40, 41], the next trial solution $\mathbf{x}^{i+1}$ is gleaned from the optimisation of the Co-Kriging model, which has been constrained to the vicinity of the current optimum solution $\mathbf{x}^*$, by the TR radius δ^i (see Table 1). At each iteration, an optimisation of the Co-Kriging model is performed within a TR, where the model trends are thought to approximate the function trend adequately for finding a step towards a solution. Once completed, the trial solution is evaluated by comparing the actual improvement in the objective function to the predicated improvement $\widehat{y}_p$. The trial step is then either accepted or rejected based on a sufficient decrease condition and the TR is updated based on the comparative performance of the model. Unlike traditional TR approaches, in this scheme all solutions rejected or otherwise,

Table 1. Trust Region Approach, where $\widehat{R}_a$, $\widehat{R}_p$ represent the Kriging and Co-Kriging model respectively and **Lb**, **Ub** are the lower and upper bounds over which the models are optimised.

begin Trust Region Approach
$\mathbf{x}_p^0 = \mathbf{x}_a^*$ **or** $\mathbf{x}_p^*$
$\mathbf{y}_p^0 = \mathbf{3dFEMSimPrimary}\left(\mathbf{x}_p^0\right)$, $[\theta_d, \rho, \lambda_d] = \mathbf{MLE}\left(\mathbf{y}_p^0, \mathbf{y}_a^0, \mathbf{x}_p^0\right)$
$\widehat{R}_p = \mathbf{CoKrigCreate}\left(\mathbf{y}_p^0, \mathbf{y}_a^0, \mathbf{x}_p^0, \theta_d, \rho, \lambda_d\right)$, $\widehat{y}_p^0 = \widehat{R}_p\left(\mathbf{x}_p^0\right)$
set $i = 0$, $\delta^0 = 0.2$, $\mathbf{Lb} = \mathbf{x}_p^0 - \delta^0$, $\mathbf{Ub} = \mathbf{x}_p^0 + \delta^0$
for $j = 1 : n_p^{tr}$
  $\mathbf{x}_p^{i+1} = \mathbf{Optimise}\left(\widehat{R}_p, \mathbf{Lb}, \mathbf{Ub}\right)$
  $\mathbf{y}_p^{i+1} = \mathbf{3dFEMSimPrimary}\left(\mathbf{x}_p^{i+1}\right)$
  $\mathbf{y}_a^{i+1} \approx \widehat{y}_a = \widehat{R}_a\left(\mathbf{x}_p^{i+1}\right)$
  $[\theta_d, \rho, \lambda_d] = \mathbf{MLE}\left(\mathbf{y}_p^{i+1}, \mathbf{y}_a^{i+1}, \mathbf{x}_p^{i+1}\right)$
  $\widehat{R}_p = \mathbf{CoKrigCreate}\left(\mathbf{y}_p^{i+1}, \mathbf{y}_a^{i+1}, \mathbf{x}_p^{i+1}, \theta_d, \rho, \lambda_d\right)$
  $\widehat{y}_p^{i+1} = \widehat{R}_p\left(\mathbf{x}_p^{i+1}\right)$
  $\zeta = \|\mathbf{y}_p^{i+1} - \mathbf{y}_p^i\| / \|\widehat{y}_p^{i+1} - \widehat{y}_p^i\|$
  if $\zeta <= 0.01$ **then** $\delta^{i+1} = \delta^i / 5$
  elseif $\zeta > 0.5$ **then** $\delta^{i+1} = \mathbf{min}\left(\delta^i * 2, 1\right)$
  else $\delta^{i+1} = \delta^i$
  endif
  if $\|\mathbf{x}_p^{i+1} - \mathbf{x}_p^i\|_2 <= 1e^{-3}$ **or** $\delta^{i+1} <= 1e^{-3}$ **then**
    return
  endif
  if $\mathbf{y}_p^{i+1} < \mathbf{y}_p^{i+1}$ **then** $i = i + 1$
  else $\delta^i = \delta^i / 5$
  endif
  $\mathbf{Lb} = \mathbf{x}_p^i - \delta^{i+1}$, $\mathbf{Ub} = \mathbf{x}_p^i + \delta^{i+1}$
end Trust Region Approach

are incorporated into the Co-Kriging model in order to improve the accuracy of the model within the expected optimum vicinity.

2. RESULTS

We now present our strategy for the geometric optimisation of NIR metamaterial structures utilising a Co-Kriging model, built from 3d full-wave numerical simulations solved at varying levels of discretisation and solver accuracy. By optimising the geometry of

artificial metallic-dielectric structures to give a specific electric and magnetic response to incident electromagnetic waves, the effective refractive index of the composite material can be varied from positive to negative. A material can have a negative refractive index if its effective permittivity and permeability satisfy the following necessary condition $\epsilon'\mu'' + \epsilon''\mu' < 0$. Along with providing the required negative index values, many metamaterial-enabled devices must have minimal absorption loss and reflection properties. Consequently, the metallic-dielectric structures must be optimised to give an electromagnetic response that simultaneously balances ϵ', μ' and ϵ'', μ'' to produce the desired negative refractive index across the frequency band of interest. The goal therefore should be to maximise the figure of merit (FOM) represented by the ratio

$$\left\| \frac{n'}{n''} \right\| = \frac{\|\epsilon'\| \, \|\mu\| + \|\epsilon\| \, \|\mu'\|}{\|\epsilon''\| \, \|\mu\| + \|\epsilon\| \, \|\mu''\|}. \tag{26}$$

Subject to this relation, it is clear that double negative NIM will result in greater values of FOM as compared to single negative NIM, where either ϵ' or μ' are negative. Incorporating this constraint into our optimisation scheme is achieved by using the constrained expected improvement as detailed in Section 1.6.

While there is no hard-and-fast rule that specifies the size of the initial sampling plan (n_a^{lhc}), it is generally accepted that a minimum value of $n^{lhc_a} > 10d$, where d is the dimension of the problem, will be required to reasonably cover the d-dimensional landscape [10, 11]. While the main benefits of Co-Kriging are achieved with increasing the number of design variables, there is of course a natural upper limit on this number. The limiting factor being the time required to tune the hyper-parameters for large quantities of data, overtaking the expense of a 3d full-wave simulation. Therefore, one must be careful to isolate only the most important design variables.

The LHC sampling technique is used in conjunction with the maximum optimality criterion of Morris and Mitchell as the initial design of experiment (DOE) sample data set. Of course the goal here is not to create a globally accurate model, but one which should be accurate enough to guide the search towards promising areas of the landscape. In order to achieve this aim in an optimal manner, we employ the LOLA-Voronoi with a minimum value of $n_a^{lv} = n_a^{lhc}$. Following this process, the location of new points of interest are iteratively found using the $\text{Max}\{E[I(\mathbf{x})] * P[F(\mathbf{x})]\}$ criteria (performed by a Hybrid Particle Swarm Optimisation algorithm (HPSO) [42]) as discussed in Section 1.6. After each iteration, the hyper-parameters are subsequently re-tuned until the global optimum is found. The optimisation of these hyper-parameters, via maximisation of the MLEs,

requires $o(n^3)$ factorisation for each evaluation of the likelihood, where n is the numbers of sample points upon which the model is constructed. The cost of this optimisation therefore increases dramatically as the number of sample points and dimension increases, resulting in a natural

Table 2. Co-Kriging algorithm, note that all design variables are normalised into the unit cube to safeguard against scaling issues.

begin Co-Kriging
$\mathbf{x}^r = [b_x^-; b_x^+, b_y^-; b_y^+, w_c^-; w_c^+, l_c^-; l_c^+, w_e^-; w_e^+, g^-; g^+, t_s^-; t_s^+]$
$\mathbf{x}_a = \mathbf{LatinHyperCube}\,(\mathbf{x}^r \rightarrow [0,1])$
$\mathbf{y}_a = \mathbf{3dFEMSimAuxiliary}\,(\mathbf{x}_a \rightarrow \mathbf{x}^r)$
for $i = 1 : n_a^{lv}$
  $\mathbf{x}_a = [\mathbf{x}_a; \mathbf{LOLAVoronoi}\,(\mathbf{x}_a, \mathbf{y}_a)]$
  $\mathbf{y}_a = [\mathbf{y}_a; \mathbf{3dFEMSimAuxiliary}\,(\mathbf{x}_a^i \rightarrow \mathbf{x}^r)]$
endfor
$[\theta_a, \lambda_a] = \mathbf{MLE}\,(\mathbf{x}_a, \mathbf{y}_a)$
$\widehat{R}_a = \mathbf{KrigCreate}\,(\mathbf{y}_a, \mathbf{x}_a, \theta_a, \lambda_a)$
for $j = 1 : n_a^{cei}/4$
  for $k = 1 : 4$
    $\mathbf{x}_a = [\mathbf{x}_a; \mathbf{CEI}\,(\mathbf{x}_a, \mathbf{y}_a)]$
    $\mathbf{y}_a = [\mathbf{y}_a; \mathbf{3dFEMSimAuxiliary}\,(\mathbf{x}_a^{\text{end}} \rightarrow \mathbf{x}^r)]$
  endfor
  $[\theta_a, \lambda_a] = \mathbf{MLE}\,(\mathbf{x}_a, \mathbf{y}_a)$
  $\widehat{R}_a = \mathbf{KrigCreate}\,(\mathbf{y}_a, \mathbf{x}_a, \theta_a, \lambda_a)$
endfor
$\mathbf{x}_a^* = \mathbf{Min}\,(\mathbf{y}_a)$
$\mathbf{x}_p = \mathbf{SubSet}\,(\mathbf{x}_a)$
$\mathbf{y}_p = \mathbf{3dFEMSimPrimary}\,(\mathbf{x}_p \rightarrow \mathbf{x}^r)$
for $j = 1 : n_p^{cei}$
  $\mathbf{x}_p = [\mathbf{x}_p; \mathbf{CEI}\,(\mathbf{x}_p, \mathbf{y}_p)]$
  $\mathbf{y}_p = [\mathbf{y}_p; \mathbf{3dFEMSimPrimary}\,(\mathbf{x}_p^{\text{end}} \rightarrow \mathbf{x}^r)]$
  $\mathbf{y}_a = [\mathbf{y}_a; \approx \widehat{y}_a = \widehat{R}_a\left(\mathbf{x}_p^j\right)]$
  $[\theta_d, \rho, \lambda_d] = \mathbf{MLE}\,(\mathbf{x}_p, \mathbf{y}_p, \mathbf{y}_a)$
  $\widehat{R}_p = \mathbf{CoKrigCreate}\,(\mathbf{y}_p, \mathbf{y}_a, \mathbf{x}_p, \theta_d, \rho, \lambda_d)$
endfor
$\mathbf{x}_p^* = \mathbf{Min}\,(\mathbf{y}_p)$
end Co-Kriging

limit on the size of n and d. In an attempt to reduce this cost, we limit the re-tuning of the auxiliary hyper-parameters θ_a and λ_a to every fourth update (with minimal impact), while the re-tuning of the primary hyper-parameters is performed at each step. The tuning of the hyper-parameters is performed by a sequential GA-SQP algorithm [43] that combines the efficiency and robustness of the global search Genetic Algorithm (GA) with the fast convergence of the Sequential Quadratic Programming algorithm (SQP). While the model accuracy can be assessed by using a leave-one-out cross validation procedure [12], this is neither a computationally efficient approach or warranted in a global optimisation routine. Instead, the maximum CEI updates should proceed starting from a small initial sample size and stop when $\mathrm{Max}\{E[I(\mathbf{x})]*P[F(\mathbf{x})]\}$ falls consecutively below a threshold over a number of iterations or when the maximum number of iterations have been met $n_a^{cei} <= 10d$. With $n_a = n_a^{lhc} + n_a^{lv} + n_a^{cei}$ in place, a conservative value of $n_e <= 10d$ should be chosen, split between a Morris-Mitchell exchange derived subset [12] (n_p^{ss}) of $\mathbf{x}_a$ and the CEI infill criteria (n_p^{cei}).

Exploitation of the Co-Kriging model can now be implemented by employing a TR inspired methodology, as outlined in Table 1 and subsequently in Table 2. This ensures accelerated convergence of the Co-Kriging scheme to a solution of the primary problem. The size of the initial trust region is set at 20% of the design space and then updated based on the design obtained from optimising the Co-Kriging model. This iterative process continues until either the trust region process converges or the maximum number of iterations has been met ($n_p^{tr} <= 2d$). For ease of implementation, the salient features of the proposed metamaterial optimisation approach can be identified in the block diagram of Figure 3.

2.1. 2D Mode Hybridisation ELC Metamaterial NIM Design (D7)

We first consider the application of the proposed topology optimisation strategy to achieve a NIR response within the K_u band (10–18 GHz) of a 2D mode hybridisation metamaterial structure as shown in Figure 1 and experimentally demonstrated in [26]. The structure is parameterised by $d = 7$ design variables whose ranges $\mathbf{x}^r$ and rankings θ are given in Table 3. While θ cannot tell us about the interaction between the variable it does provide the order of importance of the parameters. The ability to filter noise out of the model is a key attribute to the Co-Kriging approach and this is borne out in the high values of the regression factor λ_a, and to a lesser extent λ_p required to

Table 3. Relative change in the eigenfrequencies ω_{e1}, ω_{m2} subject to an increase in a single parameter, with regression constants $\lambda_a = 0.56$, $\lambda_p = 0.85$ and scaling term $\rho = 0.11$.

Symbol	Min value	Max value	θ_a	θ_d	ω_{e1}	ω_{m2}
b_x	3.7	4.5	2.17	0.02	$\Downarrow$	$\Uparrow$
b_y	5.0	7.0	11.24	5.57	$\Downarrow$	$\Longrightarrow$
l_c	11.0	13.0	3.61	3.02	$\Uparrow$	$\Downarrow$
g	0.8	1.4	0.97	1.32	$\Uparrow$	$\Uparrow$
w_c	1.0	1.4	12.57	5.96	$\Uparrow$	$\Uparrow$
w_e	0.8	1.2	6.52	8.02	$\Uparrow$	$\Uparrow$
t_s	0.8	1.4	2.02	1.36	$\Downarrow$	$\Uparrow$
t_z	0.034	-	-	-	-	-
a_x	6.0	-	-	-	-	-
a_y	13.5	-	-	-	-	-
ϵ_r	3.55	-	-	-	-	-
$\tan\delta$	0.0027	-	-	-	-	-

smooth the primary full-wave simulation results. Included also are the corresponding effects that individual parameters have on the hybrid eigenmodes ω_{e1} and ω_{m2}. The objective of this optimisation will be to maximise the overlap between the negative ϵ from $|\omega_{e1}\rangle$ and negative μ from $|\omega_{m2}\rangle$ by adjusting the ELC geometric parameters in order to maximise the FOM.

The structures substrate is a Rogers 4003 printed circuit board ($\epsilon = 3.55$, loss tangent $\delta = 0.0027$) and is coated with a 34 µm thick copper layer on both sides. Periodic magnetic and electric boundary conditions are placed in the x and y planes respectively, and a 1 mm thick air layer is placed on either side of the structure in the z plane which constitutes the effective boundaries between the metamaterial slab and air. The auxiliary data is simulated in CST Microwave Studio subject to a $1e^{-4}$ Tetrahedral mesh accuracy, evaluated using the adaptive mesh refinement and solved using a 2nd order solver. The use of this model enables quick evaluation of designs (approximately 90 seconds), allowing for an exhaustive search of the auxiliary model. Correspondingly, the primary model is discretised using $1e^{-5}$ Tetrahedral mesh accuracy and a 3rd order solver resulting in an average simulation time of 741 seconds.

Results obtained from five different optimisation strategies are outlined in Table 4, with the size of n_a fixed throughout so as to allow

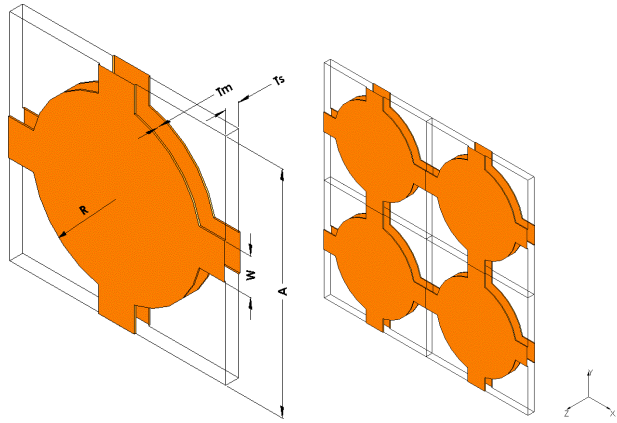

Figure 2. (a) Schematic representation of the 2D isotropic fishnet metamaterial design and (b) isometric view of a layer of the metamaterial consisting of a fishnet layer separated by a thin dielectric substrate.

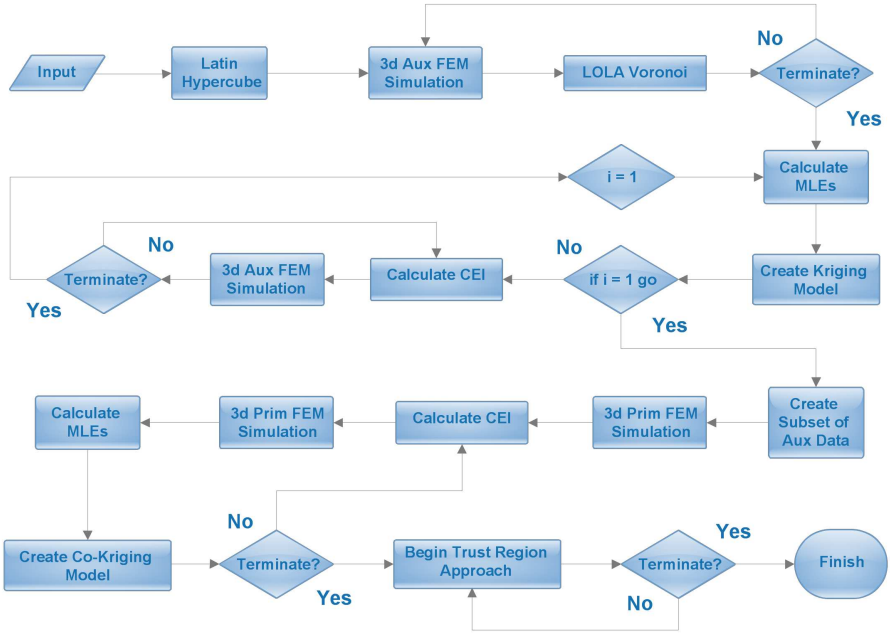

Figure 3. Block diagram of the proposed metamaterial optimisation cycle.

Table 4. Results for the 2D mode hybridisation ELC metamaterial NIM design (D7) comparing various optimisation strategies, where $n_c = n_c^{lhc} + n_c^{lv} + n_c^{cei}$, $n_e = n_e^{ss} + n_e^{cei}$ and time is given in seconds.

	V1	V2	V3	V4	V5
b_x	4.49	4.484	3.82	4.092	3.959
b_y	5.96	5.962	5.944	5.938	5.942
l_c	12.93	12.93	12.71	12.93	12.94
g	1.39	1.389	1.284	1.4	1.399
w_c	1.17	1.166	1.0	1.151	1.155
w_e	0.95	0.954	1.129	0.9852	0.9816
t_s	1.31	1.321	1.351	1.298	1.318
LHC n_a^{lhc}	70	70	140	70	70
LV n_a^{lv}	70	70	-	70	70
CEI n_a^{cei}	70	70	70	70	70
Subset n_p^{ss}	-	-	20	20	20
CEI n_p^{cei}	-	-	50	22	22
TR n_p^{tr}	1	5	6	-	10
Av. time t_c	38.2	38.2	38.2	38.2	38.2
Av. time t_e	152.6	152.6	152.6	152.6	152.6
Max. FOM	11.89	11.96	12.39	13.03	13.43
GHz	13.01	13.04	13.95	13.0	13.55
n	−1.337+0.1125	−1.205+0.10	−1.442+0.1164	−1.525+0.117	−1.531+0.114
ϵ	−1.152	−1.144	−1.433	−1.617	−1.664
	−1.538	−1.269	−1.44	−1.426	−1.398
Total Time	11675	13825	56411	26965	32454

a comparison of the results. Strategy V1 refers to Kriging, where the optimum y_a^* is used as the basis for one iteration of the primary model, likewise, V2 combines the Kriging model the TR methodology to develop an limited Co-Kriging model. V3 is an Co-Kriging model that uses a larger LHC set instead of the LOLA-Voronoi iterations, while V4 and V5 are Co-Kriging models that apply LOLA-Voronoi with and without the TR methodology.

The Co-Kriging based search consistently outperforms the Kriging based search in finding better optima. This highlights the deficiency in that the optimum of an auxiliary model would provide either a valid starting point for a trust region approach or provide the Co-Kriging with a basis for a limited design parameter range. However, the auxiliary data when coupled with a small number of primary data in a Co-Kriging model is sufficient to narrow the search towards promising areas of the landscape. It is clearly evident from the results of this paper that the LOLA-Voronoi is not just an approach to avoid sampling sub-optimal regions, but one which can produce a significant reduction in computational time as a consequence of requiring less maximum CEI global searches in determining the new sample points.

It should also be emphasized that the TR algorithm exhibits excellent convergence patterns consistently in both the V2 and V5 optimisation strategies (see Figure 4(d)) based on a very small number of primary model evaluations.

The effective medium properties of the optimum design variables ($\mathbf{x}^* = [3.959, 5.942, 12.94, 1.399, 1.155, 0.9816, 1.318]$) determined by the optimisation strategy V5 are plotted in Figures 4(a)–4(c). These dielectric properties give a complex effective refractive index of $n = -1.531 + 0.114i$ at 13.55 GHz with a FOM of 13.43 obtained in a time of 9.02 hours with 210 auxiliary simulations and a total of 54 primary model evaluations.

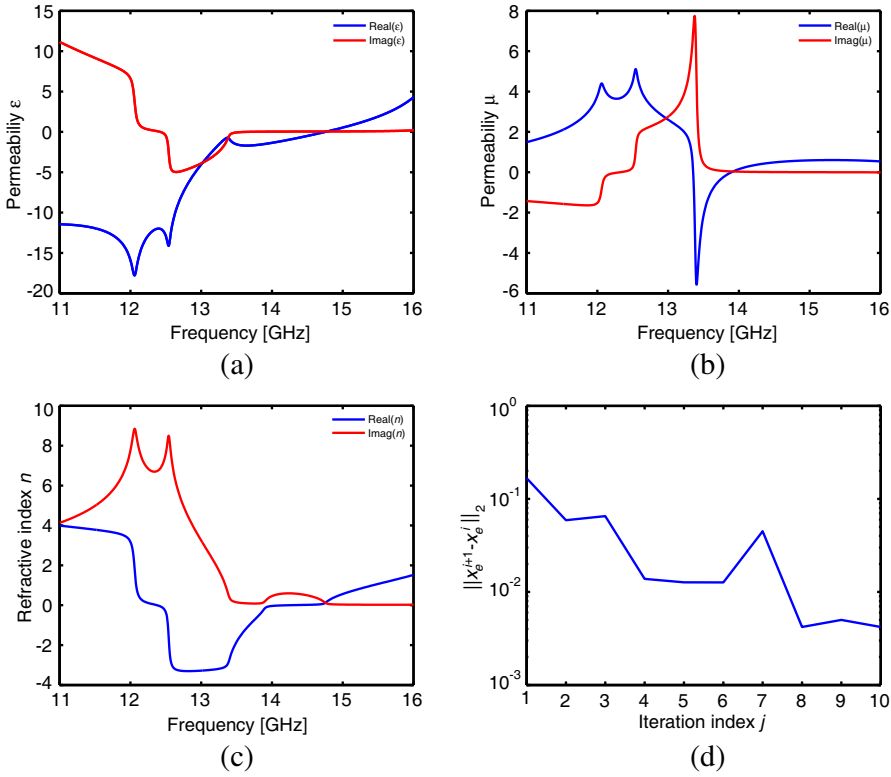

Figure 4. Example 1: Real and imaginary parts of (a) the effective permittivity, (b) permeability, (c) index of refraction, retrieved from the full-wave simulation of the metamaterial structure D7 and (d) the trust region convergence plot where the index value corresponds to the number of primary model evaluations based on $\mathbf{x}^*$ provided by the optimisation strategy V5.

2.2. 2D Isotropic Fishnet Metamaterial NIM Design (D6)

Along with providing low-loss NIR values, many metamaterial enabled devices require minimal reflection and absorption loss over a wide bandwidth. To enhance the efficiency of these NIMs, the impedance of the metamaterial should be well matched to free space and overlap with the double negative index region. In this study, we consider the application of the proposed topology optimisation strategy to achieve a polarisation independent low-loss broadband NIR of $n = -1 + 0i$ at 40 GHz, using the fishnet metamaterial structure as shown in Figure 2. This will be achieved, by optimising the geometry to give an electromagnetic response that simultaneously balances ϵ, $\mu \to -1$ at the same frequency, to produce the desired NIR response and provides a matched impedance with free space. The goal therefore should be to minimise the cost objective function

$$\text{Cost} = \|n - n_{\text{target}}\|^2 + \|z - z_{\text{target}}\|^2 . \tag{27}$$

where $n_{\text{target}} = -1 + 0i$ and $z_{\text{target}} = 1 + 0i$ are the target refractive index and relative impedance, respectively. As before, double negative NIM constraints will be incorporated into our optimisation scheme.

Table 5. Results for the 2D isotropic fishnet metamaterial NIM design (D6) comparing various optimisation strategies, where $n_c = n_c^{lhc} + n_c^{lv} + n_c^{cei}$, time is given in seconds (hours) with regression constants $\lambda_a = 3.1e-6$, $\lambda_p = 0.14$ and scaling term $\rho = 0.09$.

	V1	V2	Range	θ_a	θ_d
a	4.91	4.884	4.5⊛ 5.5	115.42	54.29
w	1.8	1.772	1.0⊛ 2.0	6.34	0.0011
r	2.07	2.096	1.5⊛ 2.5	207.56	46.71
t_s	1.17	1.189	0.6⊛ 1.2	1.72	0.001
t_m	0.01	1.01335	0.01⊛ 0.02	0.002	0.001
ϵ_r	-	-	2.2	-	-
tand	-	-	0.0009	-	-
LHC n_a^{lhc}	50	50	-	-	-
LV n_a^{lv}	50	50	-	-	-
CEI n_a^{cei}	100	100	-	-	-
TR n_p^{tr}	1	5	-	-	-
Av. time t_c	65.6	65.6	-	-	-
Av. time t_e	215	215	-	-	-
FOM$_n$	37.83	40.86	-	-	-
n	–0.98+0.0259	–0.997+0.0244	-	-	-
z	1.069-0.0154	0.981-0.0139	-	-	-
Cost	0.006	0.001	-	-	-
ϵ	–0.917	–1.017	-	-	-
m	–1.049	–0.978	-	-	-
Total Time	12826	14532	-	-	-

The structure is parameterised by $d = 5$ design variable whose ranges $\mathbf{x}^r$ and rankings θ are given in Table 5. From these values, it is clear that the period a and radius r dominate the response of the fishnet structure while the remaining parameters have little impact on the resonance. This greatly reduces the complexity of the objective function landscape and ensures that the auxiliary model needs only to be coupled with a significantly reduced number of primary model evaluations within a trust region framework in order to achieve the desired electromagnetic response.

A similar simulation setup as given in Section 2.1 is adhered too, and experimentally demonstrated in [23], resulting in evaluation times of approximately 65 and 215 seconds for the auxiliary and primary models, respectively. The unit cell substrate is a Duroid 5880 ($\epsilon = 2.2$, loss tangent $\delta = 0.0009$ at 40 GHz) separating two

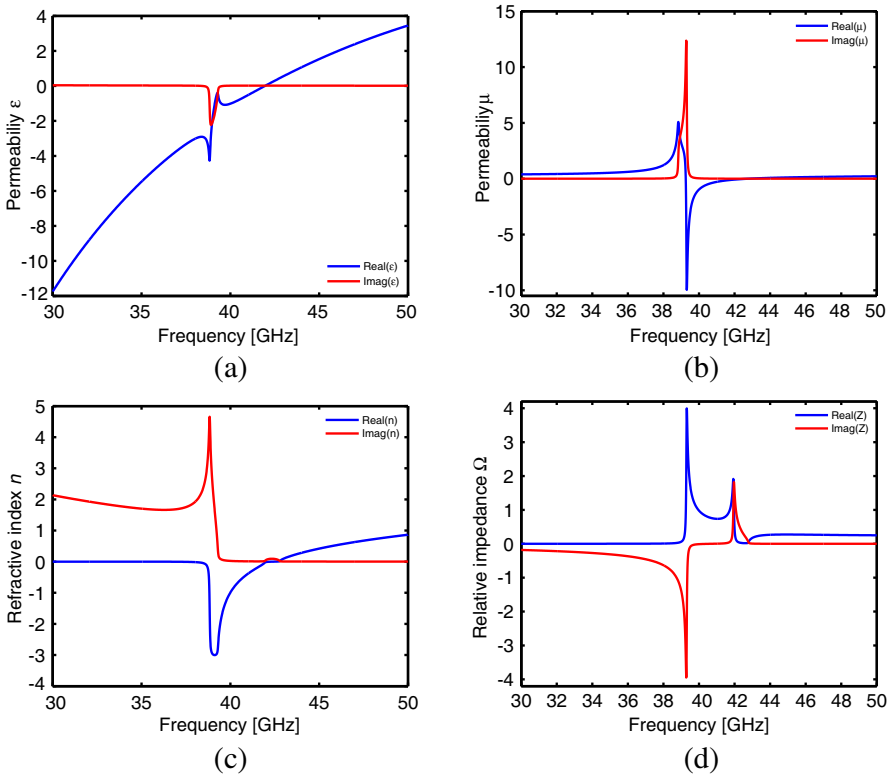

Figure 5. Example 2: Real and imaginary parts of (a) the effective permittivity, (b) permeability, (c) index of refraction, (d) relative impedance, retrieved from the full-wave simulation of the metamaterial structure D6 based on $\mathbf{x}^*$ provided by the optimisation strategy V2.

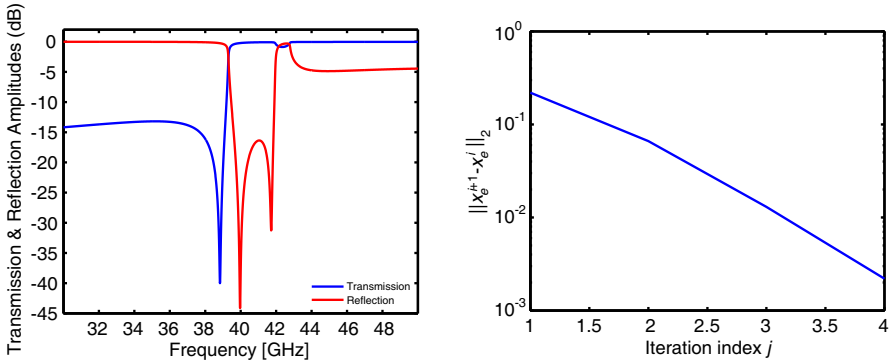

Figure 6. Example 2: (a) Reflection Γ and transmission T coefficients, trust region convergence plot where the index value corresponds to the number of (b) primary model evaluations, retrieved from the full-wave simulation of the metamaterial structure D6 based on $\mathbf{x}^*$ provided by the optimisation strategy V2.

copper layers. The termination condition parameter is set to Cost $<= 1e-3$ and as indicated above the algorithm is terminated either upon convergence or if the trust region size is sufficiently small. As can be seen in Table 5, the optimisation strategy V2 has converged to $1e-3$ after only 5 primary model evaluations within the TR framework (see Figure 6(b)). The resulting metamaterial parameters for this design $\mathbf{x}^* = [4.884, 1.772, 2.096, 1.189, 0.01335]$ are plotted in Figures 5(a)–5(d) which exhibits a double negative between 38.1 GHz and 41.8 GHz that corresponds to NIM bandwidth of 3.7 GHz. At the target frequency the near unity relative impedance ($z = 0.981 - 0.0139$) and -1 index NIR band ($n = -0.997 + 0.0244$) coupled with their respective small imaginary component, is central to the observed low reflection and absorption loss as exhibited in the transmission and reflection coefficients, Figure 6(a). For this specific optimised design the archived FOMs for the NIR and effective impedance are 40.86 and 70.57, respectively.

3. CONCLUSIONS

In this work, we proposed an efficient and automated optimisation approach, which exploits the Co-Kriging methodology in the design and optimisation of metamaterial structures. This approach overcomes the limitations of conventional approaches, such as Gradient-based and evolutionary algorithms by successfully coupling varying levels of discretisation and solver accuracy. This ensures that the computation time is drastically reduced in finding the global optimum, by proving

a more exhaustive search of the auxiliary model to seed a narrower search using the primary simulations. In addition, we investigated the improvement in efficiency of optimisation through the use of the LOLA-Voronoi, in conjunction with CEI and the embedding of a trust-region framework within our optimisation algorithm. The effectiveness of the outlined algorithm was demonstrated by a quantitative evaluation of the performance of optimised planar 2D NRI structures in the GHz regime. Future research direction includes the integration of alternative parameter retrieval extraction schemes within our optimisation framework and the investigation of including sensitivity information into the Co-Kriging model.

REFERENCES

1. Pendry, J. B., A. J. Holden, D. J. Robbins, and W. J. Stewart, "Magnetism from conductors and enhanced nonlinear phenomena," *IEEE Trans. on Microwave Theory and Techniques*, Vol. 47, No. 11, 2075–2084, Nov. 1999.
2. Smith, D. R., W. J. Padilla, D. C. Vier, S. C. Nemat-Nasser, and S. Schultz, "Composite medium with simultaneously negative permeability and permittivity," *Physical Review Letters*, Vol. 84, 4184–4187, May 2000.
3. Bradley, P. J., "Quasi-Newton model-trust region approach to surrogate-based optimisation of planar metamaterial structures," *Progress In Electromagnetics Research B*, Vol. 47, 1–17, 2013.
4. Huang, R., Z.-W. Li, L. B. Kong, L. Liu, and S. Matitsine, "Analysis and design of an ultra-thin metamaterial absorber," *Progress In Electromagnetics Research B*, Vol. 14, 407–429, 2009.
5. Koziel, S., J. W. Bandler, and Q. S. Cheng, "Robust trust-region space-mapping algorithms for microwave design optimization," *IEEE Trans. on Microwave Theory and Techniques*, Vol. 58, No. 8, 2166–2174, Aug. 2010.
6. Koziel, S. and D. Echeverra Ciaurri, "Reliable simulation-driven design optimization of microwave structures using manifold mapping," *Progress In Electromagnetics Research B*, Vol. 26, 361–382, 2010.
7. Krige, D. G., "A statistical approach to some basic mine valuation problems on the witwatersrand," *Journal of the Chemical, Metallurgical and Mining Society of South Africa*, Vol. 52, No. 6, 119–139, Dec. 1951.
8. Broomhead, D. S. and D. Lowe, "Multivariable functional interpolation and adaptive networks," *Complex Systems*, Vol. 2, 321–355, 1988.

9. Box, G. E. P. and N. R. Draper, *Empirical Model-building and Response Surface*, John Wiley & Sons, Inc., New York, USA, 1986.
10. Jones, D. R., M. Schonlau, and W. J. Welch, "Efficient global optimization of expensive black-box functions," *Journal of Global Optimization*, Vol. 13, No. 4, 455–492, Dec. 1998.
11. Jones, D. R., "A taxonomy of global optimization methods based on response surfaces," *Journal of Global Optimization*, Vol. 21, No. 4, 345–383, 2001.
12. Forrester, A., A. Sobester, and A. Keane, *Engineering Design via Surrogate Modelling: A Practical Guide*, Wiley, 2008
13. Forrester, A. I. J., A. Sbester, and A. J. Keane, "Multifidelity optimization via surrogate modelling," *Proceedings of the Royal Sociery A*, Vol. 463, No. 2088, 3251–3269, Dec. 2007.
14. Deschrijver, D., K. Crombecq, H. M. Nguyen, and T. Dhaene, "Adaptive sampling algorithm for macromodeling of parameterized S-parameter responses," *IEEE Trans. on Microwave Theory and Techniques*, Vol. 59, No. 1, 39–45, Jan. 2011.
15. Koziel, S., L. Leifsson, I. Couckuyt, and T. Dhaene, "Robust variable-fidelity optimization of microwave filters using Co-Kriging and trust regions," *Microwave and Optical Technology Letters*, Vol. 55, No. 4, 765–769, 2013.
16. Liu, R., A. Degiron, J. J. Mock, and D. R. Smith, "Negative index material composed of electric and magnetic resonators," *Applied Physics Letters*, Vol. 90, No. 26, 263504–263504-3, 2007.
17. Zhou, J., E. N. Economon, T. Koschny, and C. M. Soukoulis, "Unifying approach to left-handed material design," *Optics Letters*, Vol. 31, No. 24, 3620–3622, Dec. 2006.
18. Withayachumnankul, W., C. Fumeaux, and D. Abbott, "Near-field interactions in electric inductive-capacitive resonators for metamaterials," *Journal of Physics D: Applied Physics*, Vol. 45, No. 48, 485101, 2012.
19. Liu, H., T. Li, S. M. Wang, and S. N. Zhu, "Magnetic plasmon modes introduced by the coupling effect in metamaterials," *2008 International Workshop on Metamaterials*, 50–52, 2008.
20. Kanté, B., S. N. Burokur, A. Sellier, A. de Lustrac, and J.-M. Lourtioz, "Controlling plasmon hybridization for negative refraction metamaterials," *Phys. Rev. B*, Vol. 79, 075121, Feb. 2009.
21. Zhou, J., T. Koschny, L. Zhang, G. Tuttle, and C. M. Soukoulis, "Experimental demonstration of negative index of refraction," *Applied Physics Letters*, Vol. 88, No. 22, 221103–221103-3, 2006.
22. Zhou, J., L. Zhang, G. Tuttle, T. Koschny, and C. M. Soukoulis,

"Negative index materials using simple short wire pairs," *Phys. Rev. B*, Vol. 73, 041101, Jan. 2006.

23. Zaoui, W. S., K. Chen, W. Vogel, and M. Berroth, "Low loss broadband polarization independent fishnet negative index metamaterial at 40 GHz," *Photonics and Nanostructures — Fundamentals and Applications*, Vol. 10, No. 3, 245–250, 2012.
24. Zhang, S., W. Fan, N. C. Panoiu, K. J. Malloy, R. M. Osgood, and S. R. J. Brueck, "Experimental demonstration of near-infrared negative-index metamaterials," *Phys. Rev. Lett.*, Vol. 95, 137404, Sep. 2005.
25. Ding, P., E. J. Liang, W. Q. Hu, L. Zhang, Q. Zhou, and Q. Z. Xue, "Numerical simulations of terahertz double-negative metamaterial with isotropic-like fishnet structure," *Photonics and Nanostructures — Fundamentals and Applications*, Vol. 7, No. 2, 92–100, 2009.
26. Shen, N.-H., L. Zhang, T. Koschny, B. Dastmalchi, M. Kafesaki, and C. M. Soukoulis, "Discontinuous design of negative index metamaterials based on mode hybridization," *Applied Physics Letters*, Vol. 101, 081913, 2012.
27. Smith, D. R., D. C. Vier, Th. Koschny, and C. M. Soukoulis, "Electromagnetic parameter retrieval from inhomogeneous metamaterials," *Phys. Rev. E*, Vol. 71, 036617, Mar. 2005.
28. Nicolson, A. M. and G. F. Ross, "Measurement of the intrinsic properties of materials by time-domain techniques," *IEEE Trans. on Instrumentation and Measurement*, Vol. 19, No. 4, 377–382, 1970.
29. Varadan, V. V. and R. Ro, "Unique retrieval of complex permittivity and permeability of dispersive materials from reflection and transmitted fields by enforcing causality," *IEEE Trans. on Microwave Theory and Techniques*, Vol. 55, No. 10, 2224–2230, 2007.
30. Barroso, J. J. and U. C. Hasar, "Constitutive parameters of a metamaterial slab retrieved by the phase unwrapping method," *Journal of Infrared, Millimeter, and Terahertz Waves*, Vol. 33, No. 2, 237–244, 2012.
31. Hsieh, F.-J. and W.-C. Wang, "Full extraction methods to retrieve effective refractive index and parameters of a bianisotropic metamaterial based on material dispersion models," *Journal of Applied Physics*, Vol. 112, No. 6, 064907–064907-10, 2012.
32. Alù, A., "Restoring the physical meaning of metamaterial constitutive parameters," *Phys. Rev. B*, Vol. 83, 081102, Feb. 2011.

33. Kennedy, M. C. and A. O'Hagan, "Predicting the output from a complex computer code when fast approximations are available," *Biometrika*, Vol. 87, No. 1, 1–13, 2000.
34. Picheny, V., T. Wagner, and D. Ginsbourger, "A benchmark of Kriging-based infill criteria for noisy optimization," *Structural and Multidisciplinary Optimization*, 1–20, 2013.
35. Forrester, A. I. J., N. W. Bressloff, and A. J. Keane, "Optimization using surrogate models and partially converged computational fluid dynamics simulations," *Proceedings of the Royal Society A*, Vol. 462, No. 2071, 2177–2204, Jul. 2006.
36. Toal, D. J. J., A. I. J. Forrester, N. W. Bressloff, A. J. Keane, and C. Holden, "An adjoint for likelihood maximization," *Proceedings of the Royal Society A*, Vol. 465, No. 2111, 3267–3287, Nov. 2009.
37. Couckuyt, I., F. Declercq, T. Dhaene, H. Rogier, and L. Knockaert, "Surrogate-based infill optimization applied to electromagnetic problems," *International Journal of RF and Microwave Computer-Aided Engineering*, Vol. 20, No. 5, 492–501, 2010.
38. Morris, M. D. and T. J. Mitchell, "Exploratory designs for computational experiments," *Journal of Statistical Planning and Inference*, Vol. 43, No. 3, 381–402, 1995.
39. Sasena, M. J., "Flexibility and efficiency enhancements for constrained global design optimization with Kriging approximations," Ph.D. Thesis, University of Michigan, 2002.
40. Dennis, Jr., J. E. and R. B. Schnabel, *Numerical Methods for Unconstrained Optimization and Nonlinear Equations (Classics in Applied Mathematics*, Vol. 16, Soc. for Industrial & Applied Math., 1996.
41. Koziel, S., L. Leifsson, I. Couckuyt, and T. Dhaene, "Robust variable-fidelity optimization of microwave filters using Co-Kriging and trust regions," *Microwave and Optical Technology Letters*, Vol. 55, No. 4, 765–769, 2013.
42. Yu, S., Z. Wu, H. Wang, and Z. Chen, "A hybrid particle swarm optimization algorithm based on space transformation search and a modified velocity model," W. Zhang, Z. Chen, C. C. Douglas, and W. Tong, editors, *High Performance Computing and Applications*, Volume 5938 of *Lecture Notes in Computer Science*, 522–527, Springer, Berlin, Heidelberg, 2010.
43. Mansoornejad, B., N. Mostoufi, and F. Jalali-Farahani, "A hybrid GA-SQP optimization technique for determination of kinetic parameters of hydrogenation reactions," *Computers & Chemical Engineering*, Vol. 32, No. 7, 1447–1455, 2008.